

Study on hydrodynamic performance of Heavier-than-water AUV with overlapping grid method

Xiang Li¹, Min Zhao^{*1}, Faming Zhao², Qingqing Yuan¹ and Tong Ge¹

¹State Key Laboratory of Ocean Engineering, Shanghai Jiao Tong University, Shanghai, China

²China Ship Scientific Research Center, Wuxi, China

(Received November 7, 2013, Revised December 20, 2013, Accepted December 22, 2013)

Abstract. Hydrodynamic coefficients strongly affect the dynamic performance of autonomous underwater vehicles (AUVs). A novel kind of underwater vehicle (Heavier-than-water AUV) with higher density than water is presented, which is different from conventional ones. RANS method and overlapping grids are used to simulate the flow field around the vehicle. Lifts, drags and moments of different attack and drift angles in steady state are calculated. The hydrodynamic performances and how the forces change with the attitude are analyzed according to the flow field structure. The steady-state results using overlapping grid method are compared with those of software FLUENT and wind tunnel tests. The calculation results show that the overlapping grid method can well simulate the viscous flow field around the underwater vehicle. Overlapping grid skills have also been used to figure out the planar-motion-mechanism (PMM) problem of Heavier-than-water AUV and forecast its hydrodynamic performance, verifying its effectiveness in dealing with the dynamic problems, which would be quite helpful for design and control of Heavier-than-water AUV and other underwater vehicles.

Keywords: hydrodynamic performance; heavier-than-water AUV; overlapping grid method; planar-motion-mechanism (PMM)

1. Introduction

With the fast development of marine conservation, oceanic reconnaissance and ocean engineering, there is a growing need for various kinds of autonomous underwater vehicles (AUVs) with high performance (Bandyopadhyay 2005, Bellingham and Rajan 2007, Bovio *et al.* 2006, Desa *et al.* 2006). Novel AUVs have gradually become a research hotspot nowadays due to their advantages such as better flexibility, higher load, longer distance and lower cost, etc (Wang *et al.* 2012).

However, most conventional submersibles have neutral buoyancy and need to carry bulky adjusting device of buoyancy during navigation. This feature makes conventional submersibles not only consume too much energy, but also have bad flexibility and motion performance.

In this paper, a new type of submersible, Heavier-than-water AUV (HTW for short), having capability of cruising with negative buoyancy is proposed as a bold attempt (Yan 2012). Just carrying a few small devices (or even nothing at all) for buoyancy adjusting and without huge

*Corresponding author, Assistant Researcher, E-mail: min.zhao@sjtu.edu.cn

buoyancy parts, its size is much smaller and its cruising range can be extended much larger than that of conventional ones. Its motion performance like speed and mobility can also be improved obviously at the same time.

With great improvement of numerical technology in computational fluid dynamics (CFD) and rapid development of computer hardware, CFD technology gradually goes into the stage of practical engineering. In the actual flow, the shapes of objects are always very complicated. How to effectively deal with complex surface boundaries and generate meshes of high quality, is still one of the most important topics in CFD technology at present.

Although unstructured grid and Cartesian rectangular grid have gradually become popular nowadays, structured grid is still the good choice of viscous flow calculation due to its mature technology, strong ability of simulating viscous wall, smaller resultant numerical dissipation with less expansion ratio in space, etc. In order to make better use of the advantages of structured grid, people are eager to develop quick generation methods of structured grids which would be convenient and easy for complex configuration. Hence generation method of block structured grids appeared. But when solving grids of objects with several appendages, this method needs good grid techniques and is so complex that it is difficult to really solve quick generation technique of structured grids. In addition, commercial software (such as Gambit, ICEM) has powerful function in unstructured grid, multi-block structured grid and dynamic grid. There would be much more work with commercial software when simulating six degrees of freedom movement (especially greatly motor problems), multi-body relative motion and motion in restricted conditions, etc. If appendages and boundary restrictions are taken into consideration, CFD simulation will be more difficult. The appearance of overlapping grid (or chimera grid, overset grid) makes the generation of structured grids much easier. The structured grids of an object with several appendages can be generated more conveniently and the motion problem will be solved more easily. Far field background grid uses a Cartesian rectangular grid, all the bodies and appendages use body-fitted grids. Information is delivered through interpolation between background grid and body-fitted grid, as well as through body surface overlapping (detailed skills are showed in 3.2). So the CFD simulation problems of structured grids with appendages and moving bodies can be figured out easily through overlapping grid method. Application of overlapping grid method in ocean engineering has got much attention during these years. There are already several research on surface vessels with overlapping grid method (Tahara *et al.* 2006, Kandasamy *et al.* 2011). And maneuvering performance of surface vessels including planar mechanism motion, turn and zigzag maneuvers was studied with overlapping grids during the few years (Simonsen *et al.* 2008, Carrica *et al.* 2012, Sakamoto *et al.* 2012a, Sakamoto *et al.* 2012b). And for underwater vehicle and submarine, Boger and Dreyer (2006) predicted the hydrodynamic forces and moments for several underwater vehicles using overset grids. Chase and Carrica (2013) simulated the DARPA Suboff submarine including self-propulsion with the E1619 propeller using the overset flow solver.

As a novel kind of underwater vehicle, the Heavier-than-water AUV has a pair of wings, learned from characteristics of aircraft navigation. Without depending on buoyancy, HTW makes use of the fluid lift during navigation to balance the surplus weight under water. With the shape of an airplane, it has both the characteristics of submersible and aircraft. This paper mainly introduces the body surface overlapping technique and applies it in the static and dynamic computation of HTW with overlapping grids thus getting a full comprehension of the hydrodynamic performance of HTW.

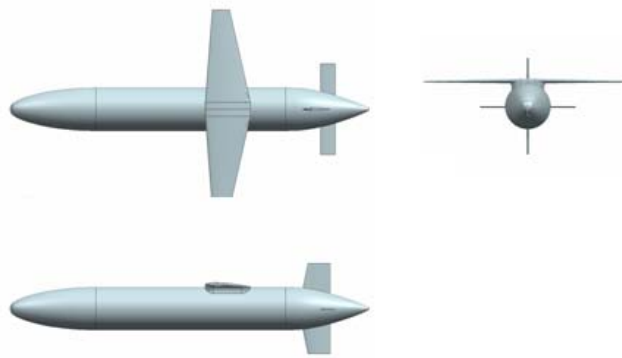


Fig. 1 Heavier-than-water AUV in three views

2. Heavier-than-water AUV

As a new type of underwater vehicles, the navigation performance of Heavier-than-water AUV (HTW) in the water is different from the others, which is determined by its configuration characteristics and working environment. HTW has negative buoyancy and needs to get lift from its wings in order to balance the surplus weight in the water. In view of this special demand, HTW has a different structure and shape from traditional submersibles and its three views is displayed in Fig. 1.

The Heavier-than-water AUV, Flying Fish II, is taken as an example and its hydrodynamic and movement performance is analyzed in this paper. Its design parameters are showed in Table 1.

Heavier-than-water AUV mainly consists of four parts (Yan 2012)

(1) Main hull

To reduce resistance, main hull is shaped as a streamlined torpedo body. Necessary equipments and mechanisms are laid out internally, mainly including energy system, control system and so on, in order to meet the navigation and operation requirements.

(2) Wing

When HTW is sailing in the water, the lift is resulted from the relative speed between water flow and the wing, which is perpendicular to direction of the aerofoil chord length. When HTW smoothly flies at the cruising speed, the joint lift in the vertical direction produced by wing, main hull and tails equals the total weight in the water.

(3) Appendages

Appendages refer to parts exceeding HTW's streamline shape, including tails, stem rudders, external sensors, auxiliary equipments, etc. As the main parts of appendages, the tails are direction control actuators of HTW, divided into horizontal tails and vertical tails.

Horizontal rudders are installed on horizontal tails, whose rotation angles are changed to balance trimming moment produced by the wing and control the navigation attitude of longitudinal motion; Vertical rudders are installed on vertical tails, whose rotation angles are changed to adjust heading to ensure direction stability in the horizontal plane. HTW can also control its rolling motion through differential action of rudder angles.

(4) Propulsion system

Propulsion system is an important part of HTW. From the outside, propulsion system is beyond the streamline shape and may be considered as attached. As propulsion system isn't included in the wind tunnel test model, its influence on the flow field around and the stress state of HTW wasn't considered in our calculation. But as an independent function system, propulsion system's control characteristics and installation method have an important effect on the voyage performance of HTW. So it will be an independent part to be considered separately in addition.

Table 1 Design parameters of Flying Fish II

Diameter (m)	0.19	Total length(m)	1.6
Weight in the air(kg)	62	Weight in the water (kg)	22
cruising speed (kn)	6	Working depth (m)	100

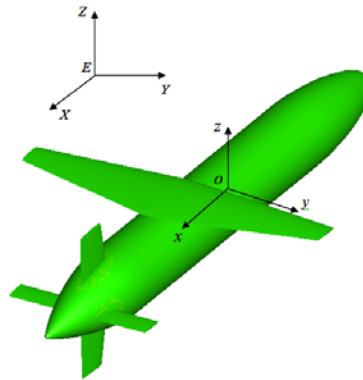


Fig. 2 Definition of coordinate system and symbols

3. Overlapping grid method

3.1 Brief introduction to overlapping grid method

Overlapping grid method can divide complex flow area into subdomains with simple geometric boundary. Grid of each independent subdomain is generated separately, with overlapping, nested or covering relations. The flow field information is exchanged and matched through the interpolation at the boundary of overlapping regions. Structured grid can describe the flow field with simple logical relationship, high precision and efficiency, strong ability of simulating viscous wall etc. But overlapping method can make up for structured grid's weakness of the shape adaptive capacity at the same time. In recent years overlapping grid technology develops with continuous innovation and wide application rapidly. There are already famous foreign overlapping codes, like PEGASUS of NASA, SUGGAR and SUGGAR++ of Celeritas Simulation Technology, LLC, OVERTURE (Rogers 2012, Rogers *et al.* 2003).

The ultimate goal of overlapping grid method is to establish the coupling relationship between overlapping grids, helping different grid subdomain exchange boundary information for flow field calculation. The generation of overlapping grids does not simply equal to the combination of child

grids. The more important thing is to determine the overlapping relation and interpolation transitive relation between the subgrids. So overlapping grid method contains two major steps: hole cutting and interpolation.

Hole cutting means masking some unnecessary or meaningless data (such as internal part of object walls) from the grids before flow field calculation. To be specific, holes need to be cut around the masking area, and then the grid points that fall into the holes are marked. Marked points are useless and will be abandoned in further computation. Hole cutting methods can be divided into designated hole surface method, hole mapping method and tree method is adopted in this paper, hole mapping method.

Searching points refers to searching for donor cells of the interpolation points. The simplest and the most reliable method is to go through the entire grid domain until finding the right grid cell. But this kind of method has the lowest efficiency, whose searching speed would be quite slowly for larger grid data. A good data structure can improve the searching velocity by orders of magnitude. There are also several common methods of searching points, like stencil walk method, inverse map method, tree method and ADT (alternating digital tree) method. ADT method is adopted in this paper.

3.2 Body surface overlapping

Generally, overlapping region appears in the boundary area of far field with the information exchanges between donor and receptor being done in the volumetric space. But grids are not wanted overlapped on the body surface, because overlapping body surface in the boundary layer with big flow field gradient will bring errors to calculation. But for complex grids of an underwater vehicle with appendages complex, overlapping grids are preferred in the body surface where boundary layers exist to reduce the difficulty of structured grid generation. In the generating process of body surface overlapping grids, grids including body surfaces can be generated independently. But as a result of difference in factors like geometric error, surface curvature resolution and smoothness between different surfaces, the so-called "mismatch" problem that the described body surface is non-unique in the overlapping region will be caused, as shown in Fig. 3. From the figure, we can see that some points can't find their donor cells. Or some can find donor cells, but far from body surface, thus producing a large error and affecting accurate calculation of the flow field.

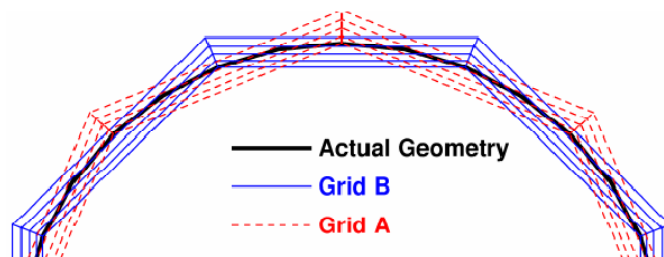


Fig. 3 Mismatch of 2D surface grids

In order to avoid the above errors due to surface overlapping, Petersson (1999) did research on the mismatch of wall boundaries. He proposed the use of a global variable ε to represent tolerance of boundary mismatch, and gave the equation of mismatch tolerance to balance the influence of surface boundary mismatching on trilinear isoparametric interpolation. Overlapping code, PEGASUS5 of NASA, adopts mutual projection technique to solve the mismatching problem of body surfaces based on PROGRD code (Rogers *et al.* 2003, Petersson 1999, Paterson *et al.* 2003).

A similar projection method is also used in this paper. As shown in Fig. 4, point P_s and point P belong to grid A, and get donor cells from grid B. The first step is to project P_s to grid B with projection vector $\vec{\varepsilon}$. The second step is to calculate the distance δ_1 between point P and point P_s . Modified point P^* is obtained with $\vec{\varepsilon}$ and δ_1 from Eq. (1), and is only used to calculate interpolation coefficient without changing the original grid points (Schwarz *et al.* 2010). Overlapping grids of HTW with appendages using above method is shown in Fig. 5.

$$\vec{X}_{P^*} = k \cdot \vec{\varepsilon} + \vec{X}_P \quad (1)$$

where

$$k = \begin{cases} 1 & 0 \leq |\vec{X}_P - \vec{X}_s| < d_1 \\ \frac{d_2 - |\vec{X}_P - \vec{X}_s|}{d_2 - d_1} & d_1 \leq |\vec{X}_P - \vec{X}_s| < d_2 \\ 0 & d_2 \leq |\vec{X}_P - \vec{X}_s| \end{cases} \quad (2)$$

$$d_1 = 10|\vec{\varepsilon}|, \quad d_2 = 30|\vec{\varepsilon}|$$

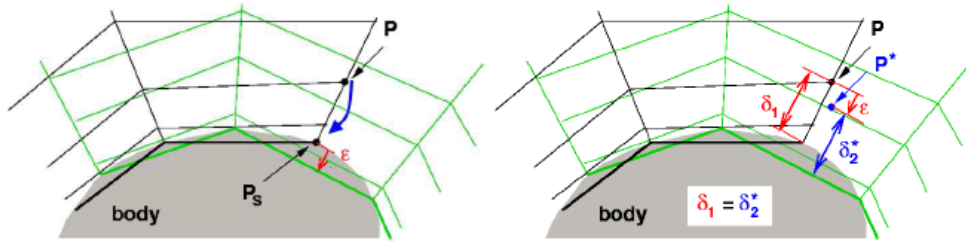


Fig. 4 Projection method of surface grids, left: projection of surface point P_s which is closest to interpolation point P onto surface of overlapping mesh; right: calculation of virtual target point P^* [20]

3.3 Overlapping grids of Heavier-than-water AUV

Heavier-than-water AUV consists of main hull, wing, horizontal and vertical tails. Overlapping grid method is to generate body-fitted grids of above components separately to ensure grid quality. There is a background grid outside with Cartesian coordinates in addition. The overlapping grids of HTW are shown in Figs. 6 and 7. In order to compare the calculation results of overlapping

grids with those by software FLUENT, block structured grids are also generated by preprocessing software ICEM as shown in Fig. 8.

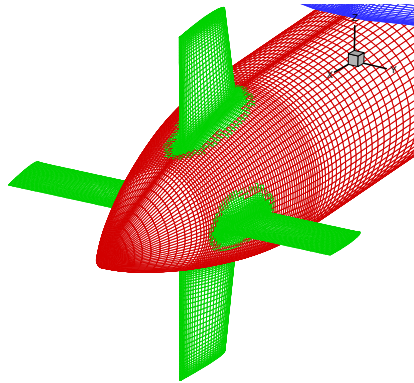


Fig. 5 Surface overlapping grids of HTW's stern

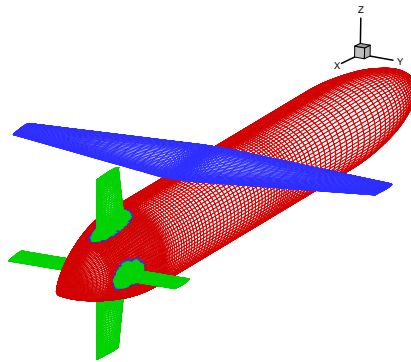


Fig. 6 Surface grids of HTW

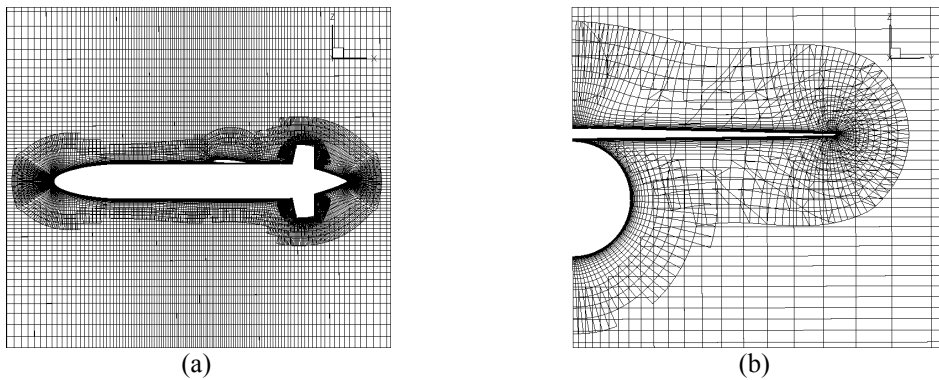


Fig. 7 Overlapping grids. (a) At the plane of symmetry and (b) At the cross section of $x=0.6$

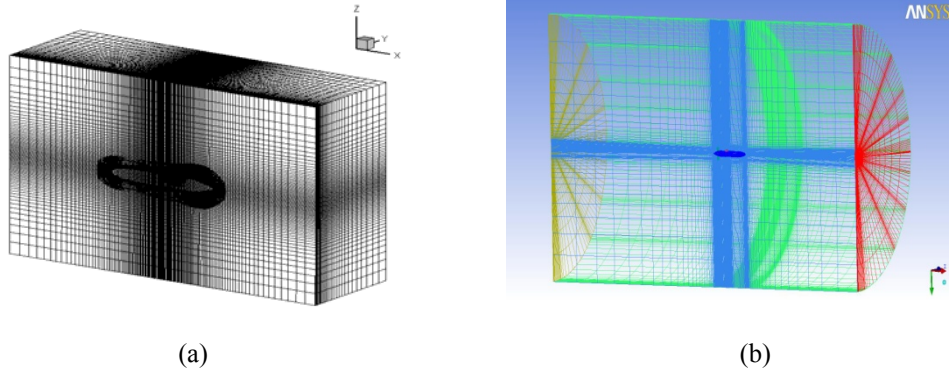


Fig. 8 Half model grids of HTW. (a) Overlapping grids and (b) Block structured grids of ICEM

4. Basic theory and numerical method

4.1 Governing equations

The Reynolds Averaged Navier Stokes (RANS) equation of three dimensional incompressible fluid is used for governing equations. The tensor forms of continuity equation and dimensionless RANS equation for incompressible fluid are as follows respectively

$$\frac{\partial u_i}{\partial x_i} = 0 \quad (3)$$

$$\frac{\partial u_i}{\partial t} + u_j \frac{\partial u_i}{\partial x_j} = -\frac{\partial p}{\partial x_i} + \frac{1}{\text{Re}_{\text{eff}}} \frac{\partial^2 u_i}{\partial x_j \partial x_j} + \frac{\partial v_t}{\partial x_j} \left(\frac{\partial u_i}{\partial x_j} + \frac{\partial u_j}{\partial x_i} \right) + s_i \quad (4)$$

where the dimensionless pressure is $p = p_{\text{abs}} / (\rho U_0^2) + 2k / 3$, and p_{abs} is the absolute pressure. The effective Reynolds number is $\text{Re}_{\text{eff}} = 1 / \text{Re} + \nu_t$.

4.2 Turbulence model

The SST $k-\omega$ two-equation turbulence model is used to solve the RANS equation. k equation of the turbulent kinetic energy and ω equation of the specific dissipation rate are as follows:

$$\frac{\partial k}{\partial t} + (u_j - \sigma_k \frac{\partial v_t}{\partial x_j}) \frac{\partial k}{\partial x_j} - \frac{1}{R_k} \nabla^2 k + s_k = 0 \quad (5)$$

$$\frac{\partial \omega}{\partial t} + (u_j - \sigma_\omega \frac{\partial v_t}{\partial x_j}) \frac{\partial \omega}{\partial x_j} - \frac{1}{R_\omega} \nabla^2 \omega + s_\omega = 0 \quad (6)$$

where the turbulent viscosity is $\nu_t = \frac{k}{\omega}$ and the Peclet numbers are defined as

$$R_k = \frac{1}{1/\text{Re} + \sigma_k v_t}, R_\omega = \frac{1}{1/\text{Re} + \sigma_\omega v_t} \quad (7)$$

4.3 Discrete method

The governing equation is discretized with cell centered finite difference scheme in space. And the time term is discretized with second order Euler backward difference scheme

$$\frac{\partial \phi}{\partial t} = \frac{1}{\Delta t} (1.5\phi^n - 2\phi^{n-1} + 0.5\phi^{n-2}) \quad (8)$$

The convection term is discretized using the second-order upwind difference scheme, and viscous term uses second-order central difference scheme. Discrete equations are solved with ADI method and PISO algorithm.

4.4 Simulation of planar-motion-mechanism

There are two kinds of motion in the planar-motion-mechanism (PMM) tests (Chislett and Strøm-Tejsen 1965): translation ones and rotation ones according to motion characteristics. Vertical PMM tests include heave motion and pitch motion as shown in Fig. 9, and their motion characteristics and data processing method are described in the below. The same method of processing data is appropriate for horizontal PMM as well, including sway motion and yaw motion.

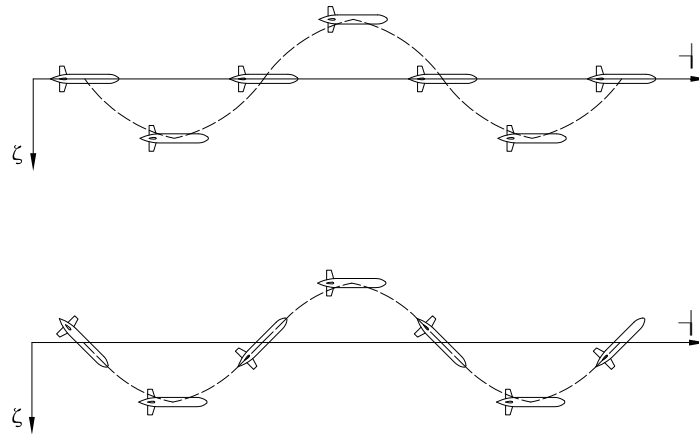


Fig. 9 Illustration of PMM tests corresponding to forward motion together with heave oscillation (top) and pitch oscillation (bottom) to determine hydrodynamic coefficients

Take the heave motion test as the example of translation motion

$$\begin{cases} \zeta = a \sin(\omega t) \\ w = \dot{\zeta} = a\omega \cos(\omega t) \\ \dot{w} = -a\omega^2 \sin(\omega t) \\ \theta = \dot{\theta} = 0 \end{cases} \quad (9)$$

Where ζ is the vertical displacement, a is the amplitude of heave motion, ω is the circular frequency of heave motion, w and \dot{w} is the vertical velocity and acceleration, θ and $\dot{\theta}$ is the angle and angular velocity about the y axis.

Take the pitch motion test as the example of rotation motion

$$\begin{cases} \theta = \theta_0 \sin(\omega t) \\ q = \dot{\theta} = \theta_0 \omega \cos(\omega t) \\ \dot{q} = -\theta_0 \omega^2 \sin(\omega t) \\ \zeta = \dot{\zeta} = 0 \end{cases} \quad (10)$$

Where θ and $\dot{\theta}$ is the angle and angular velocity about the y axis, θ_0 is the amplitude of pitch motion, ω is the circular frequency of pitch motion, q and \dot{q} is the angle velocity and acceleration, ζ and $\dot{\zeta}$ is the vertical displacement and velocity.

The parameters have already been nondimensionalized with inlet velocity of 1 m/s and characteristic length L . Every motion period is divided into 140 time steps during the calculation. Simulation calculation lasts 6~7 cycles to get periodic curves of force and moment with time without consideration of the oscillation at the beginning. The data of the last three cycles is used for post-processing.

Based on the significance of hydrodynamic coefficients, the force and moment for heave motion can be written as follows

$$Z = Z_{\dot{w}} \dot{w} + Z_w w + Z_0 = -a\omega^2 Z_{\dot{w}} \sin(\omega t) + a\omega Z_w \cos(\omega t) + Z_0 \quad (11)$$

$$M = M_{\dot{w}} \dot{w} + M_w w + M_0 = -a\omega^2 M_{\dot{w}} \sin(\omega t) + a\omega M_w \cos(\omega t) + M_0 \quad (12)$$

Where Z is the vertical force, M is the moment about the y axis.

According to Eqs. (11) and (12), the series of discrete data points are processed with Fourier transform using software MATLAB, and then the relevant hydrodynamic coefficients are derived for each motion of PMM tests.

5. Wind tunnel test

The experimental model of Heavier-than-water AUV is made and tested in the low turbulence wind tunnel of NWPU (Northwestern Polytechnical University) in Xi'an, China. The fluid force and moment coefficients of corresponding states were got in the experiment. The prototype of HTW—Flying Fish II is also built, for which the torque balance thruster is designed. The tank test

is also carried out to validate the HTW's performance of large cruising range.

The test model is made in a ratio of 1:2 compared to real size, adopting a combination structure of steel and wood. Its center of gravity keeps consistent with that of the real vehicle. Three views and key parameters of the test model are shown in Fig. 1 and Table 2 respectively.

The low turbulence wind tunnel (LTWT) located in NWPU has two layouts: separate experimental section of three units and tandem experimental section of two and three units. The minimum turbulence degree of experimental section is 0.02%. The test is taken in the experimental section of three units in LTWT, with the size of 2.8 m (length) \times 1.2 m (width) \times 1.05 m (height).

The experimental Reynolds number is about 1.102×10^6 corresponding to the characteristic length of total hull length when wind speed is 20 m/s. 10kg professional balance of $\Phi 12$ from NWPU is used to measure forces. Test contents include longitudinal test and yaw test: (1) Longitudinal experimental condition: $V = 20 \text{ m/s}$; $\alpha = -5 \sim 8^\circ$, $\Delta\alpha = 1^\circ$; (2) Yaw experimental condition: $V = 20 \text{ m/s}$; $\alpha = -2 \sim 8^\circ$, $\Delta\alpha = 2^\circ$; $\beta = -10 \sim 10^\circ$, $\Delta\beta = 2^\circ$.

In the wind tunnel test, HTW is supported with a single point at the tail (as shown in Fig. 10), forming an instable structure with heavy mass and low rigidity. Thus HTW is easily vulnerable to vibration which has a bad effect on the experimental results. Learned from this, the future work will have a great improvement from it.

Table 2 Parameters of underwater vehicle's wing

Wing's reference area S (mm^2)	30700	Full span length l (mm)	433
span-chord ratio λ	6.1	Taper ratio η	0.38
Congestion index($\alpha = 8^\circ$)	1.48%	Averaged aerodynamic chord length b_A (mm)	87

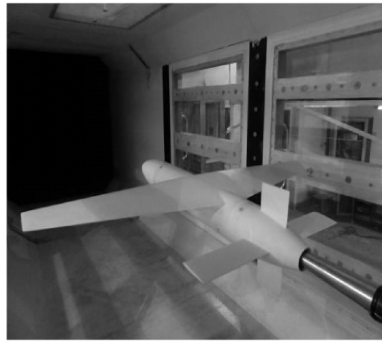


Fig. 10 Model tests in the low turbulence wind tunnel

6. Results and discussions

6.1 Simulating steady-state tests

Based on overlapping method, the flow field around Heavier-than-water AUV in infinite water depth is simulated. The Reynolds number is $Re = 1.102 \times 10^6$, similar to that of the wind tunnel

test.

For case with only attack angles, half model is used for calculation in this paper. As for grids, background grid uses Cartesian grid $150 \times 30 \times 75$, body-fitted grids of main hull and appendages use O-type grids. Total grid number is 1051214, wall function isn't used in the calculation and $y^+ \approx 0.5$. For case with attack and drift angles at the same time, the whole model is adopted which can be got from half model symmetrically.

The hydrodynamic performance of HTW at different attack and drift angles is discussed at the navigation speed of 0.727 m/s with SST $k-\omega$ turbulence model.

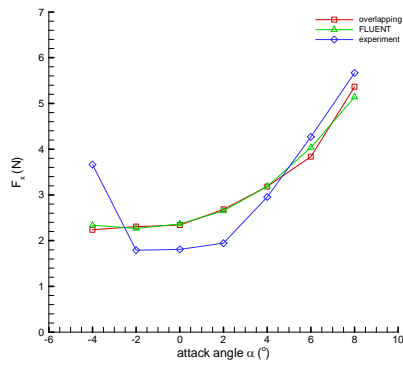


Fig. 11 Drag-attack angle curves (drift angle 0°)

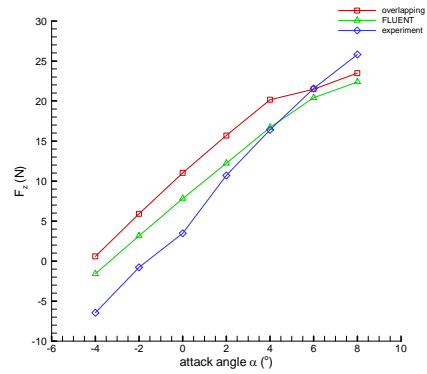


Fig. 12 Lift-attack angle curves (drift angle 0°)

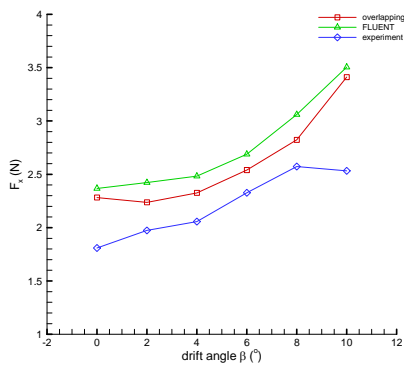


Fig. 13 Drag-drift angle curves (attack angle 0°)

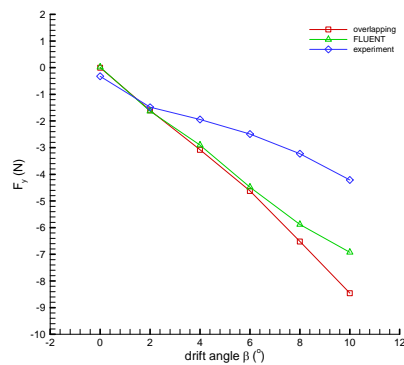


Fig. 14 Swaying force-drift angle curves (attack angle 0°)

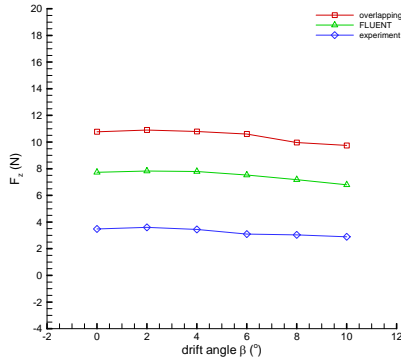


Fig. 15 Lift-drift angle curves (attack angle 0°)

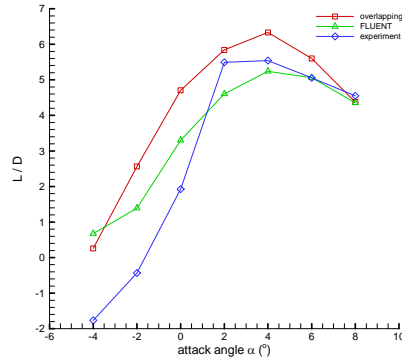


Fig. 16 Lift drag ratio-attack angle curves (drift angle 0°)

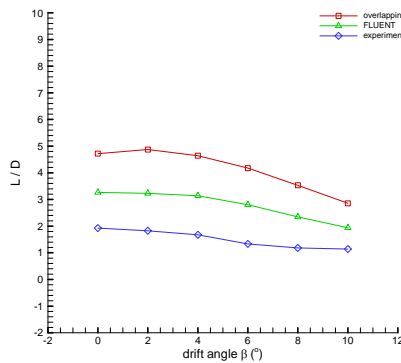


Fig. 17 Lift drag ratio-drift angle curves (attack angle 0°)

Figs. 11 and 12 describe the relationships of attack angle with resistance and lift. From the chart, it is known that the calculated values with overlapping method are almost consistent with those by FLUENT, but differ slightly from those of the experiment.

There is a little large difference between the calculated lift and experimental value. The reason may be that the lift in the z direction is quite sensitive to the airfoil profile, a little difference of wing camber as a result of mesh shape error can cause bad effect on the lift. But because the lift of z direction has a closer relation with attack angle, we can see that the lift difference value at different attack angles is almost a fixed value. So the results can be considered reasonable, but have a little larger numerical difference.

Figs. 13 -15 describe the relationships of drift angle with resistance, swaying force and lift. The resistance and lift is positive, but swaying force is negative in the defined coordinates of this paper, which is in accordance with the real situation. Although existing some difference, the calculated

values with overlapping method are close to and present the same trend with those of software FLUENT and experiments in numerical value. So the calculated results can be thought reasonable.

Figs. 16 and 17 show the relationships of lift-drag ratio with the attack angle and drift angle. As shown in the graph, the calculated values of lift-drag ratio with overlapping method have a similar trend to those of software FLUENT and experiments, but the numerical results are larger than experimental ones, probably owing to low measurement accuracy in the wind tunnel test to some degree. In Fig. 17 of lift drag ratio-drift angle curves, the results of lift-drag ratio with three methods differ larger. With the increase of attack angle, lift-drag ratio first increases, and then decreases, and all three methods get the maximum ratio at the attack angle of 4 ° or so. With the increase of the drift angle, lift-drag ratio is gradually reduced.

Forces between numerical computation and experiment with both attack and drift angles at the same time are also compared. The resistance results, namely f_x in Table 3, have the least difference between overlapping and experimental values, with the maximum difference of 26.16%. The swaying forces have the larger difference, and the lift results get the largest. But the forces at larger attack and drift angles get closer computation results than those at small angles.

Table 3 Force comparison between computation and experiment with attack and drift angles

(alpha,beta)	$f_x(N)$			$f_y(N)$			$f_z(N)$		
	Overlapping	experiment	Δ^*	Overlapping	experiment	Δ	Overlapping	experiment	Δ
(-2,-2)	2.2915	2.5871	-0.1143	1.5648	1.7811	-0.1214	5.8080	-2.2102	-3.6279
(0,0)	2.2828	1.8094	0.2616	0.0004	-0.3245	-1.0012	10.7720	2.4901	3.3260
(2,2)	2.6185	2.2772	0.1499	-1.6035	-1.6179	-0.0089	15.6734	11.4393	0.3701
(4,4)	3.2455	4.3275	-0.2500	-3.2414	-1.9986	0.6218	19.9645	17.7574	0.1243
(6,6)	4.2615	5.6632	-0.2475	-4.0843	-2.7719	0.4735	21.9034	20.2810	0.0800

* $\Delta = (f_{overset} - f_{experiment}) / f_{experiment}$, f_x, f_y, f_z is the force in x, y, z direction respectively.

6.2 Simulating unsteady-state tests

With overlapping grid and numerical methods as described in Chapter 3 and 4, standard maneuvering tests of PMM are carried out to get the hydrodynamic coefficients of HTW. The hydrodynamic coefficients are obtained with $U_0 = 1m/s$ and small oscillations with frequency $f = 1.4Hz$. The amplitude of pure heave and pure sway is 0.016 m, and the amplitude of pure pitch and pure yaw is 2.5 degree. The force and moment coefficients are shown in Figs. 18 - 21.

From Figs. 20 and 21, severe shocks can be seen in the first period of the data curve. In order to avoid big errors, data processing begins from the second cycle. As we know, acceleration derivatives can only be calculated by dynamic PMM tests and they should be obtained via Fourier analysis. Thus hydrodynamic coefficients are gained with the Fourier method described in 4.4 and presented below in Table 4.

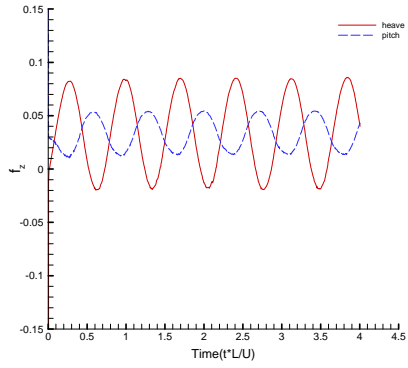


Fig. 18 Heave force coefficients vs time

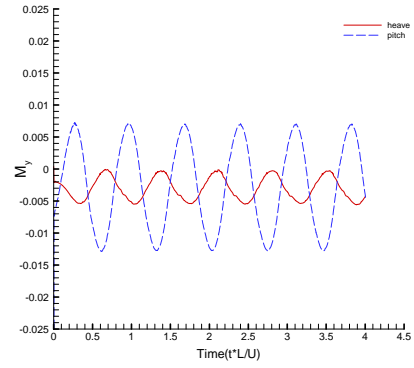


Fig. 19 Pitch moment coefficients vs time

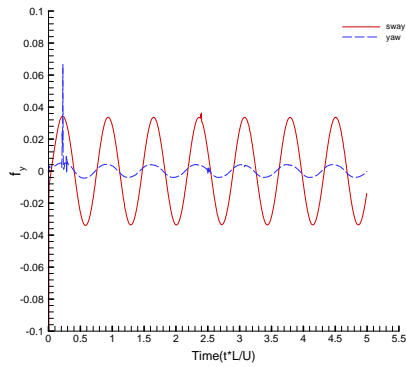


Fig. 20 Sway force coefficients vs time

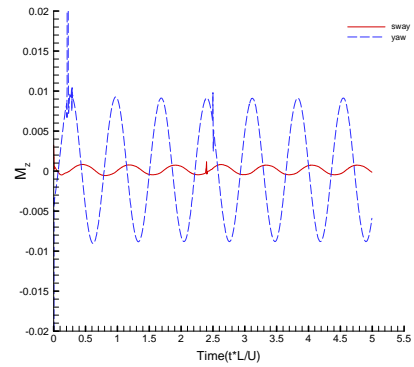


Fig. 21 Yaw moment coefficients vs time

Table 4 Calculated hydrodynamic coefficients

coefficient	value	coefficient	value
$Z_{\dot{w}}$	-0.17251	$Z_{\dot{q}}$	0.08522
Z_w	-0.18097	Z_q	0.00496
$M_{\dot{w}}$	0.00579	$M_{\dot{q}}$	-0.03820
M_w	0.01208	M_q	-0.01993
$Y_{\dot{v}}$	-0.13547	Y_r	-0.01691
Y_v	-0.05055	Y_r	0.00384
$N_{\dot{v}}$	0.00196	N_r	-0.03248
N_v	-0.00243	N_r	-0.02427

On the other hand, linear derivatives can be calculated by either static or dynamic PMM tests. Polynomials can be used to fit experimental and computational results of static PMM tests, and then the coefficients of their first-order term can be reported as a linear derivative. The longitudinal test and yaw test have been carried out in the wind tunnel. HTW has a streamlined configuration of bilateral symmetry but up-down asymmetry, so we can infer that the swaying force Y and yawing moment N are odd functions of lateral velocity v , but the heaving force Z and pitching moment M are not odd functions of vertical velocity w . In order to get the fitting function from the experimental results, third-order polynomials are used to fit the discrete points based on least square method with the `cftool` command in MATLAB (shown in Fig. 22), and then the slope value of the fitting curve at zero is calculated, thus obtaining the corresponding hydrodynamic coefficients. Hydrodynamic coefficient comparison between numerical and experimental results is shown in Table 5.

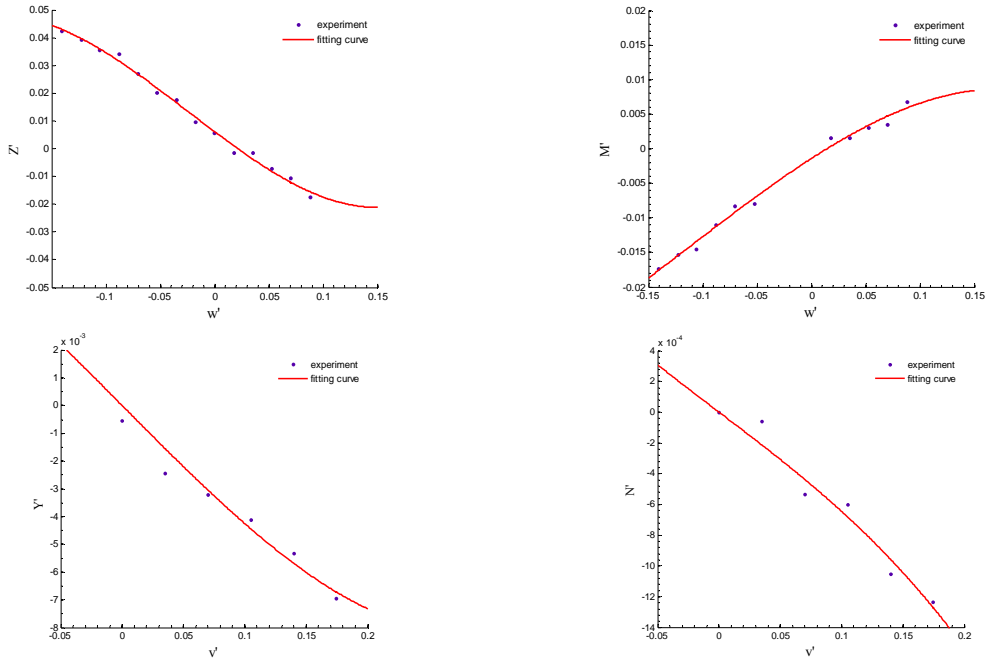


Fig. 22 Experimental dimensionless force and moment coefficient vs velocity and fitting curve

Table 5 Hydrodynamic coefficient comparison between numerical and experimental results

coefficient	CFD value	Experimental fitting value	Δ
Z_w	-0.18097	-0.29330	-38.30%
M_w	0.01208	0.10130	-88.08%
Y_v	-0.05055	-0.04455	13.46%
N_v	-0.00243	-0.00606	-59.84%

Note: $\Delta = (\text{CFD value} - \text{Experimental fitting value}) / \text{Experimental fitting value}$.

From Table 5, it is seen that Z_w , Y_v and N_v is negative representing the resistance and ability of returning to original position, validating accuracy of this calculation qualitatively. And the difference between overlapping method computation and experimental fitting value also seems acceptable.

The error of hydrodynamic coefficients exists but the results still have the value of reference. The sources of error may be various, like data processing, mesh density and quality and turbulence model, etc. There are not enough experimental data points for curve fitting as shown in Fig. 22 as a result of elimination of some points with big error, which has a negative influence on the hydrodynamic coefficient comparison. Based on the coefficients presented in Table 4, other coefficients can be derived according to correlative article.

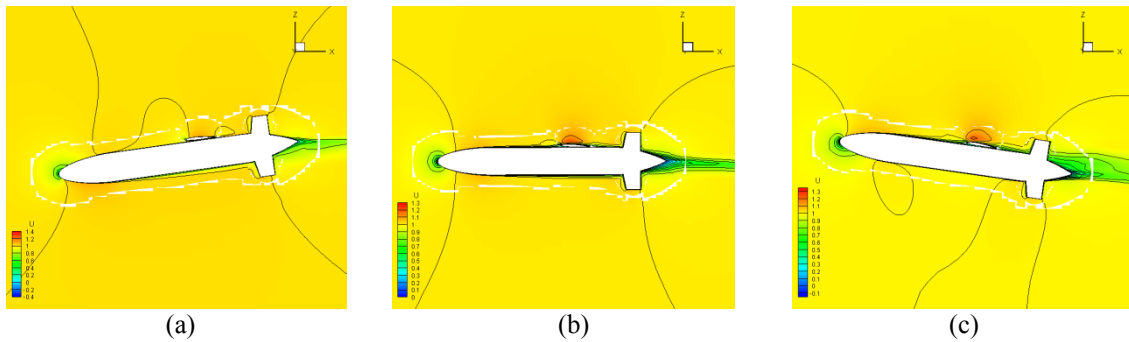


Fig. 23 Contours of velocity in the x direction around HTW with different attack angles. (a) -8° , (b) 0° and (c) 8°

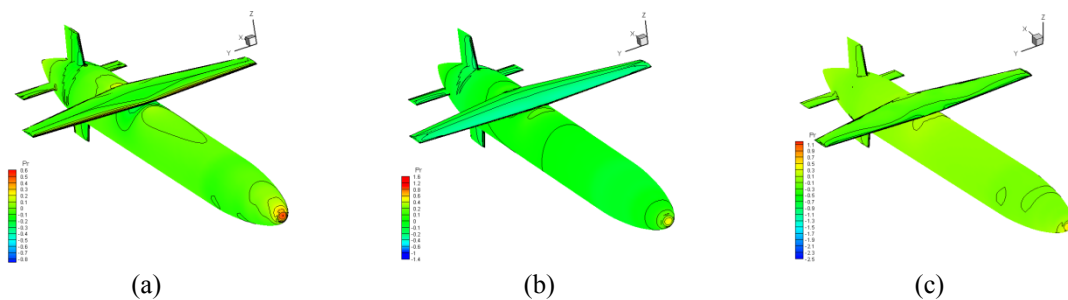


Fig. 24 Surface pressure contours of HTW with different attack angles. (a) -8° , (b) 0° and (c) 8°

Fig. 23 shows the contour map of velocity in the x direction. As shown, the flow field around HTW is obvious, and the flow velocity above the wing is higher, but at the head and leading edges of the wing and tails towards the flow is much lower. The velocity isolines in overlapping region get smooth transition, thus showing that data transfer between the overlapping grids is correct.

Fig. 24 gives the surface pressure distribution contours of HTW at different attack angles. At the head and leading edges of the wing and tails just towards the flow, the pressure values are much larger than other parts, which is consistent with the actual situation. And with the increase of

attack angle, high pressure area and pressure values changes accordingly.

7. Conclusions

Overlapping grid method is mainly used to solve RANS equation with $k-\omega$ model, cell centered finite difference scheme and PISO algorithm, and the flow field around the Heavier-than-water AUV is successfully simulated in this paper. The calculated values of resistance and lift have a small difference from values of software FLUENT and wind tunnel tests. The velocity isolines in overlapping region get smooth transition, showing that data transfer and interpolation between the overlapping grids is reasonable and effective.

Overlapping grid method is a kind of practical CFD methods and its advantages lie in efficient grid division and dynamic calculation. If the underwater vehicle moves and changes its attitude, grids don't need to be generated once again. The only thing to do is to generate interpolation information between overlapping grids, and then solve the equation of motion. Overlapping grid skills have been used to figure out the PMM problems and forecast the hydrodynamic performance of HTW, verifying its effectiveness in dealing with the dynamic problems.

Static experiment results from the wind tunnel tests have already been obtained in this paper. We have to admit that there are several shortages in need of improvement in the tests. The future work is that a series of model experiments like PMM, zigzag, rotating arm test and other self-propulsion tests in towing tank will be performed to compare with the numerical results of dynamic simulation with overlapping grid method, in order to get a systematic and comprehensive understanding of the hydrodynamic performance of Heavier-than-water AUV. We will also apply overlapping grid method to simulate the flow field around underwater vehicles with six degree of freedom motion in practical engineering in the complex motion state and complex environmental condition in the future.

Acknowledgements

The support of National Natural Science Foundation of China (Grant No. 51109132), and the Specialized Research Fund for the Doctoral Program of Higher Education of China (Grant No. 20110073120015) for this work is gratefully acknowledged.

References

- Bandyopadhyay, P.R. (2005), "Trends in biorobotic autonomous undersea vehicles", *IEEE J. Oceanic Eng.*, **30**(1), 109-139.
- Bellingham, J.G. and Rajan, K. (2007), "Robotics in remote and hostile environments", *Science*, **318**(5853), 1098-1102.
- Boger, D. and Dreyer, J. (2006), "Prediction of hydrodynamic forces and moments for underwater vehicles using overset grids", *Proceedings of the 44th AIAA aerospace sciences meeting*, Reno, Nevada.
- Bovio, E., Cecchi, D. and Baralli, F. (2006), "Autonomous underwater vehicles for scientific and naval operations", *Annu. Revi. Control*, **30**(2), 117-130.
- Carrica, P.M., Ismail, F., Hyman, M., Bhushan, S. and Stern, F. (2013), "Turn and zigzag maneuvers of a surface combatant using a URANS approach with dynamic overset grids", *J. Marine Sci. Technol.*,

- 18(2), 166-181.
- Chase, N. and Carrica P.M. (2013), "Submarine propeller computations and application to self-propulsion of DARPA Suboff", *Ocean Eng.*, **60**, 68-80.
- Chislett, M.S. and Strøm-Tejsten, J. (1965), *Planar motion mechanism tests and full-scale steering and manoeuvring predictions for a mariner class vessel*, Technical Report Hydro-and Aerodynamics Laboratory, Lyngby, Denmark.
- Desa, E., Madhan, R. and Maurya, P. (2006), "Potential of autonomous underwater vehicles as new generation ocean data platforms", *Current science*, **90**(9), 1202-1209.
- Kandasamy, M., Ooi, S.K., Carrica, P.M., Stern, F., Campana, E.F., Peri, D., Osborne, P., Cote, J., Macdonald, N. and de Waal, N. (2011), "CFD validation studies for a high-speed foil-assisted semi-planing catamaran", *J. Marine Sci. Technol.*, **16**(2), 157-167.
- Paterson, E.G., Wilson, R.V. and Stern, F. (2003), *General-purpose parallel unsteady rans ship hydrodynamics code: CFDSHIP-IOWA*, IHR Technical Report No. 432.
- Petersson, N.A. (1999), "An algorithm for assembling overlapping grid systems", *SIAM J. Sci. Comput.*, **20**(6), 1995-2022.
- Rogers, S.E. (2012), PEGASUS user's guide, <http://people.nas.nasa.gov/~rogers/pegasus/uguide.html>.
- Rogers, S.E., Suhs, N.E. and Dietz, W.E. (2003), "PEGASUS 5: An automated preprocessor for overset-grid computational fluid dynamics", *AIAA J.*, **41**(6), 25-51.
- Sakamoto, N., Carrica, P.M. and Stern, F. (2012), "URANS and DES simulations of static and dynamic maneuvering for surface combatant: part 1. Verification and validation for forces, moment and hydrodynamic derivatives", *J. Marine Sci. Technol.*, **17**(4), 422-445.
- Sakamoto, N., Carrica, P.M. and Stern, F. (2012), "URANS simulations of static and dynamic maneuvering for surface combatant: part 2. Analysis and validation for local flow characteristics", *J. Marine Sci. Technol.*, **17**(4), 446-468.
- Schwarz, T., Spiering, F. and Kroll, N. (2010), "Grid coupling by means of Chimera interpolation techniques", *Proceedings of the 2nd Symposium of Simulation of Wing and Nacelle Stall*, Braunschweig, Germany.
- Simonsen, C.D., Otzen, J.F., Joncquez, S. and Stern, F. (2013), "EFD and CFD for KCS heaving and pitching in regular head waves", *J. Marine Sci. Technol.*, (in press).
- Tahara, Y., Wilson, R.V., Carrica, P.M. and Stern, F. (2006), "RANS simulation of a container ship using a single-phase level-set method with overset grids and the prognosis for extension to a self-propulsion simulator", *J. Marine Sci. Technol.*, **11**(4), 209-228.
- Wang, Q., Ge, T., Wu, C. and Yan H. (2012), "Design of the HUV based on the airplane's principles", *Ocean Eng.*, **30**(2), 143-149 (in Chinese).
- Yan, H. (2012), *Investigation on design, navigation and motion performance of a Heavier-than-water AUV*, Ph. D. Dissertation, Shanghai Jiaotong University, Shanghai (in Chinese).